Influence of temperature processing on the microstructure and hardness of the 420 stainless steel produced by hot pressing

A. Cunha, A. Marques, M. Gasik & B. Trindade

Taylor & Francis
Taylor & Francis Group

Check for updates

Influence of temperature processing on the microstructure and hardness of the 420 stainless steel produced by hot pressing

A. Cunha [a,b], A. Marques [a,b], M. Gasik [c], and B. Trindade [d]

aCMEMS – Center for Microelectromechanical Systems, University of Minho, Azurém, Guimarães, Portugal; bLABBELS – Associate Laboratory, Braga/Guimarães, Portugal; cSchool of Chemical Engineering, Aalto University Foundation, Espoo, Finland; dCEMMPRE – Center for Mechanical Engineering, Materials and Processes, University of Coimbra, Rua Luís Reis Santos, Coimbra, Portugal

ABSTRACT

In this study, samples of 420 stainless steel were obtained by hot pressing from powder at temperatures from 1,100 to 1,200°C. The aim was to explore the influence of the processing temperature on their grain size, microstructure, densification and mechanical properties. The results showed that it is possible to produce dense samples at these sintering temperatures. The sintering temperature influenced the density, grain size, structural phases, and hardness of the samples. Martensite and austenite were present in the samples sintered at 1,100, 1,150, and 1,180°C. Precipitation of $Cr_{23}C_6$ was observed after sintering at 1,200°C. This sample was the one with the highest density (99.7% densification) and hardness (771.9 HV).

Introduction

Martensitic stainless steels are characterized by high strength and hardness and have been used in different fields such as: surgical instruments, razor blades, bearings, the marine and aerospace industries, plastic injection molds, among others.[1–3] In particular, martensitic stainless steels with a high chromium content (more than 11 wt.%), such as 420 stainless steel, provide high mechanical and corrosion properties.[4–7] The martensite structure is responsible for the strength and hardness of this steel alloy, while the chromium alloying element ensures its corrosion resistance.[8] In the annealed state, 420 stainless steel offers good ductility while after quenching exhibits excellent strength and hardness.[9,10]

Powder metallurgy is a near-net-shape manufacturing technique that consists of the consolidation of powders into a predefined shape and that provides the metallurgy integrity and mechanical resistance of the parts manufactured.[11–13] Therefore, this manufacturing method is an alternative to conventional processes such as casting, forging, or extrusion.[8,13] Despite the higher costs of the metal powders necessary, in relation to cast and wrought parts, the saving in post-processing steps (machining operations) and scrap generation makes powder metallurgy techniques very competitive.[13–15] Among all the powder metallurgy techniques (compaction step): injection molding, hot isostatic pressing, hot pressing, extrusion, and rolling stand out.[13,15] The hot pressing technique especially, characterized by the simultaneous application of temperature and uniaxial pressure, makes it possible to obtain high performance, well-consolidated components due to the high densification (through the rearrangement and deformation of particles) and, consequently, the low porosity that it confers to the final parts.[16,17] Only one study about the hot pressing of 420

stainless steel may be found in the literature.[8] In that study, the microstructure, hardness, and uniaxial mechanical response of a ball-milled 420 stainless steel powder sintered by hot pressing were assessed. The 420 stainless steel powder was consolidated in a graphite die at a temperature of 960°C by means of a pressure of 60 MPa for 400 s. The hot-pressed material had a porosity of 0.7% and was formed by a martensitic lath structure, with carbides at the grain boundaries. Barlow et al.[18] analyzed the influence of the austenitising temperature (1,000–1,200°C) on the as-quenched microstructure and mechanical properties of two 420 stainless steels with 0.5 wt.% C and different content of alloying elements. The authors concluded that the austenitising temperature influences the martensite transformation range and the retained austenite content. Therefore, the austenitising temperature plays an important role in the mechanical behavior of 420 stainless steel by controlling the partitioning of the alloying elements between the austenite and carbides.

The present study combines the knowledge available in the literature to optimize the production of 420 stainless steel parts by hot pressing. The aim is to analyze the influence of the sintering temperature on the microstructure, grain size, fracture surface, and hardness of hot-pressed 420 stainless steel.

Materials and methods

Powder

In this study, samples were produced using spherical 420 stainless steel powder supplied by Carpenter Additive (United Kingdom). The chemical composition of this steel alloy is presented in Table 1. The powder was analyzed by scanning electron microscopy (SEM) by using Nano-SEM –

Table 1. Chemical composition of 420 stainless steel powder (according to the manufacturer).

Element	C	S	P	Fe	O	N	Mn	Cr
wt. %	0.22	0.004	0.015	Balance	0.02	0.09	0.29	13.5

FEI Nova 200 equipment and dynamic light scattering (Mastersized 300, Malvern) (Fig. 1). The particles are spherical with $d_{50} = 19.6\,\mu m$. The crystal phases were determined by X-ray diffraction (×RD) using a PANalytical X'Pert PRO MPD apparatus with Co-Kα 1. 89010 A (Fig. 2). The powder is composed by martensite (α') and austenite (γ).

Hot pressing

Four different 420 stainless steel samples ($\oslash = 14\,mm$, t = 3 mm) were produced by Hot Pressing (HP) at temperatures from 1,100 to 1,200°C (75 and 83% of the melting temperature, respectively), pressure of 50 MPa and dwell time of 30 min (Table 2). The heating rate was 100°C/min.

The hot pressing was conducted using a vacuum pressure-assisted sintering system (under a vacuum of 10^{-2} mbar) with a high-frequency induction furnace (schematic representation in Fig. 3). The graphite die was positioned inside the chamber, where both pressure and temperature were increased till reaching the targeted values. These conditions were maintained during the dwelling stage.

Characterization methods

The samples of the sintered 420 stainless steel were analyzed by SEM, electron dispersive spectroscopy (EDS) (EDAX – Pegasus X4 M), XRD (PANalytical X'Pert PRO MPD with Co Kα radiation) for the structural and phase analyses, respectively.

The microstructure was assessed in different regions of the samples, i.e. at the periphery, half distance between the periphery and the center (3.5 mm from the periphery) and at the center (7 mm from the periphery). Prior to the observations, the samples were polished using silicon carbide abrasive papers with successive grades till 4,000 mesh and then cloth polished using 0.5 μm diamond suspension. After polishing, the samples were etched with Vilella's reagent for microstructural analysis. The samples were etched for 10 s to reveal the grain size and 20 s for the microstructure assessment. An optical microscope (ZEISS Imager.Z2 m) was used for the observations. The grain size was measured through the intercept technique and ten measurements were taken for each case. The density of the samples was determined by measuring their mass and volume. The percentage of densification was inferred from the theoretical and calculated density values.

The fracture surface was examined at the cross-section of the samples by SEM analysis. The Vickers hardness was evaluated with a micro-hardness tester (model 4551, Shimadzu, Quioto, Japan) with a maximum load of 2,000 gf. Seven indentations (1 mm apart) were made in each sample (from the periphery to the center) under an applied load of 100 gf and a dwell time of 15 s. The average hardness of the samples was evaluated from 10 indentations all over the surface with a load of 1,000 gf and the same dwell time.

The uncertainty of the hardness measurements was calculated according to EN ISO 6507-1:201 (procedure with bias). Five HV2 indentations were performed (maximum load of the equipment). The testing machine bias plus the expanded uncertainty was 5.6HV2 and the bias was 4.2HV2. Five hardness tests on a calibrated test block of steel with a hardness of 250 HV were performed prior to hardness measurements of the samples. Two scales were used, HV0.1 and HV1. The standard deviations of the measurements were 2.7 HV (1%) for the lowest applied load and 2.2 HV (0.9%) for the highest one.

Results and discussion

Grain size

Figure 4 shows the optical micrograph images of the four samples sintered at different temperatures. Three different areas were analyzed: periphery, halfway between the periphery and the center and at the center. The corresponding grain size was calculated, and the results are plotted in Fig. 5.

All the samples are quite dense, and no significant number of pores were detected. The joint analysis of Figs. 4 and 5 allows us to conclude that, as expected, an increase in the temperature leads to an increase in the grain size. There is a significant increase in the grain size for sintering temperatures from 1,100 to 1,180°C due to the higher driving force for the grain growth at higher temperatures (higher
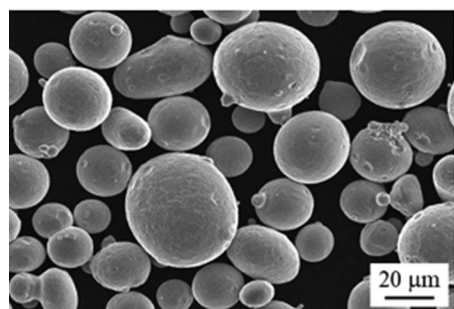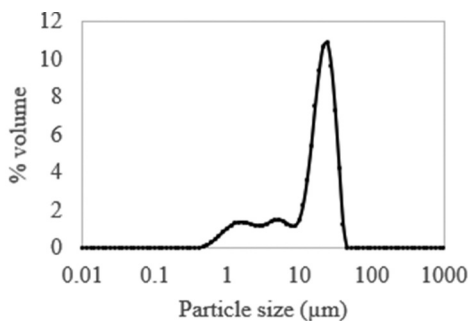
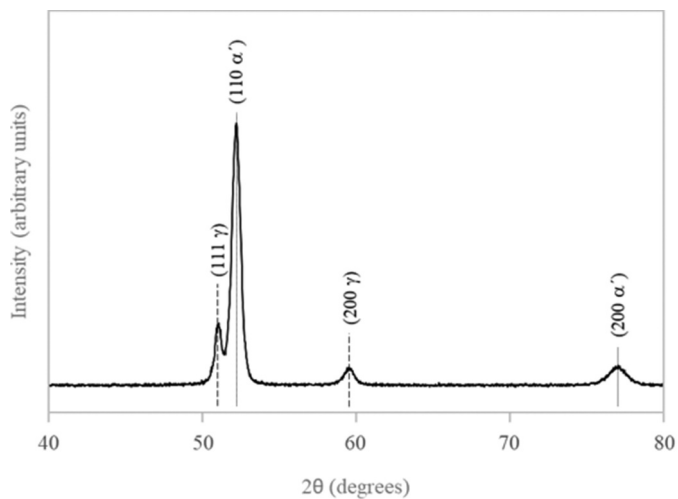**Figure 1.** 420 stainless steel powder: (a) SEM image and (b) particle size distribution.

Figure 2. XRD of 420 stainless steel powder.

Table 2. Sample code and sintering parameters.

Sample code	Sintering parameters			
	Temperature (°C)	Pressure (MPa)	Dwell time (min.)	Heating rate (°C/min)
420SS_1,100	1,100	50	30	100
422SS_1,150	1,150	50	30	100
420SS_1,180	1,180	50	30	100
420SS_1,200	1,200	50	30	100

diffusivity) and dissolution of chromium carbides at the grain boundaries. The grain size remained almost constant between 1,180 and 1,200°C, which means that all the carbides were dissolved in the matrix up to 1,180°C. Moreover, for the same sintering temperature coarser microstructures were observed at the periphery of the samples. Heat transmission takes place from the periphery to the center of the samples, so that in the total sintering cycle the surface is at a higher temperature than the center for a longer time. This explains the results obtained.
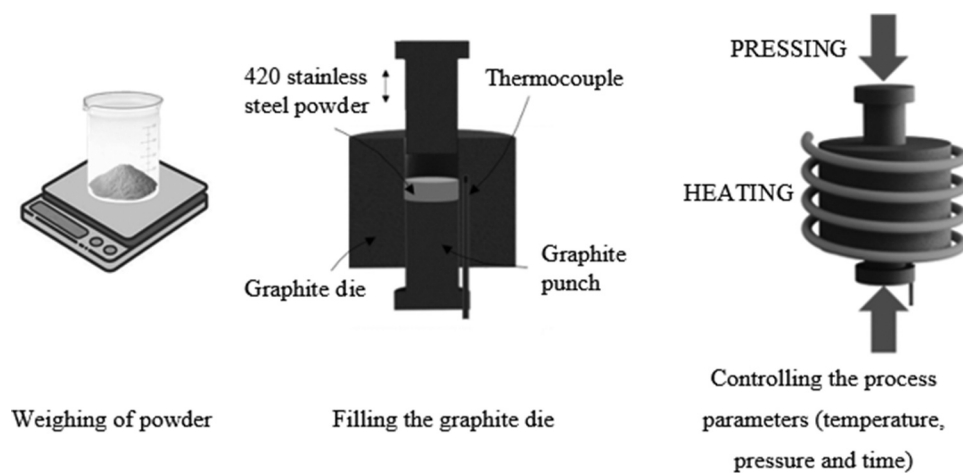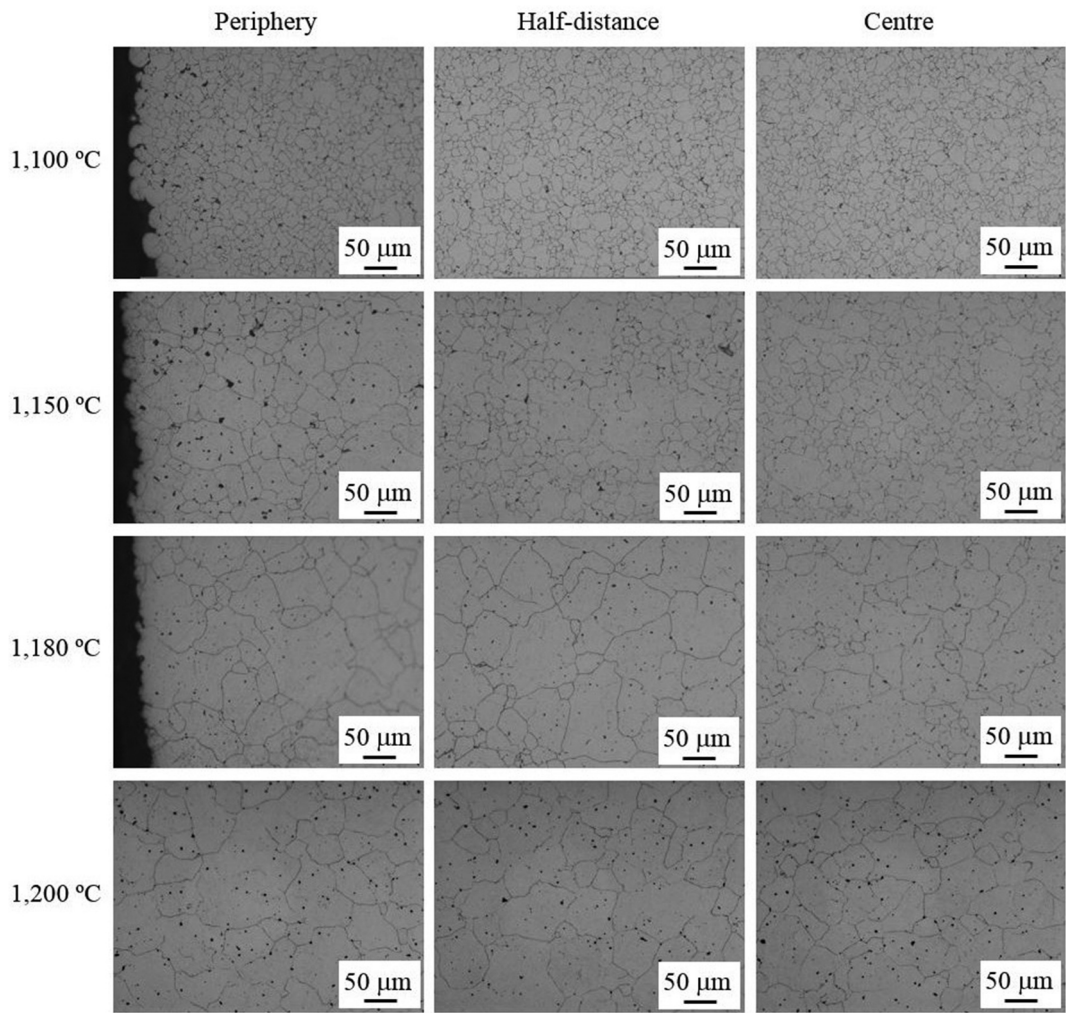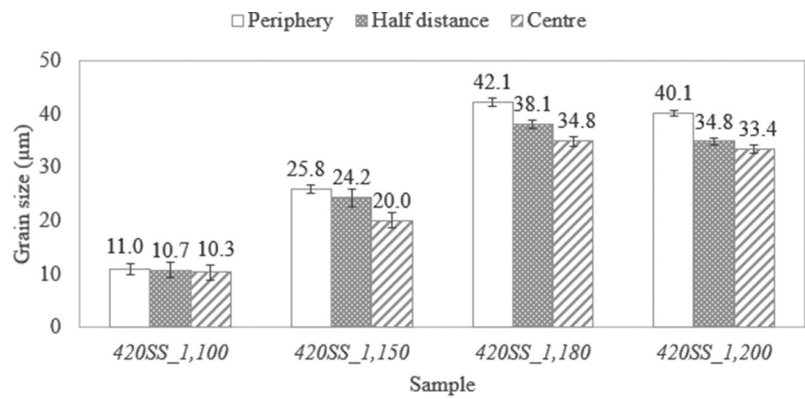
Microstructure

The optical micrographs of the microstructure of the samples are shown in Fig. 6. Figure 7 presents the XRD patterns of the samples after polishing.

The microstructures of the samples sintered at 1,100, 1,150 and 1,180°C consist mainly of martensite and small amounts of retained austenite. The same microstructure was obtained by Nachum et al. [8] in a sample of the same steel hot-pressed at 960°C. Compared to the 420 stainless steel powder, the (111) and (200) peaks of the retained austenite (γ) of the samples are less intense which means a low amount of this phase. For these samples, the peaks of the martensite phase are shifted to the left (higher lattice parameters). This shift is more significant for higher sintering temperatures. No peaks of chromium carbides were detected by X-ray diffraction for these sintering temperatures. For T = 1,200°C there is a notable change in the microstructure. The austenite peak (111) is shifted to smaller diffraction angles and the opposite happens for the (110) peak of the martensite. These results can be discussed in terms of the phases existing at the different maximum sintering temperatures. Thermodynamic predictions (using the CALPHADTM model) for the equilibrium phase diagrams show that a single austenite phase should exist at the different sintering temperatures used in this work.[18] Therefore, during cooling, a transformation from austenite to martensite should take place for high cooling rates. This was confirmed in the present study. The increase of the martensite lattice parameter observed for the samples sintered from 1,100 to 1,180°C means a variation in its chemical composition, probably due to the dissolution of any possible chromium carbides existing in the raw powder. The fact that they were not detected by X-ray diffraction does not mean that they do not exist in small amounts in the microstructure of the initial powder. Considering this hypothesis, partial or total dissolution of these carbides might have occurred at these sintering temperatures, with the incorporation of carbon and chromium in the austenite lattice and the consequent increase of the martensite lattice parameters after cooling. However, this possible dissolution

Figure 3. Schematic representation of the manufacturing process using the hot pressing technique.
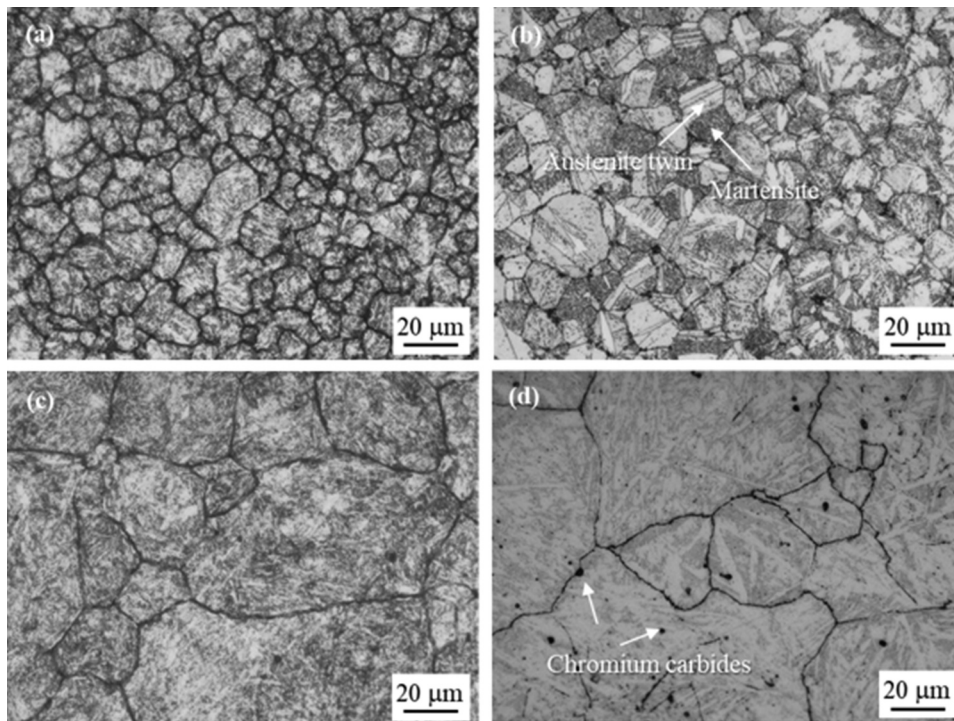
Figure 4. Optical micrograph images of the periphery, half-distance and center of the samples processed at 1,100, 1,150, 1,180 and 1,200°C.

Figure 5. Grain size along the radius of the samples processed at 1,100, 1,150, 1,180 and 1,200°C.

Figure 6. Optical micrographs showing the microstructure of the sintered samples: (a) 420SS_1,100, (b) 420SS_1,150, (c) 420SS_1,180, and (d) 420SS_1,200.

of the chromium carbides did not inhibit the martensite transformation, since no higher levels of retained austenite were observed for higher sintering temperatures.

For 1,200°C, the (110) diffraction peak is shifted to the right and its position seems to indicate the presence of ferrite rather than martensite. This agrees with the presence of $Cr_{23}C_6$

carbide in the final microstructure of this sintered sample. At this temperature, and according to the thermodynamic predictions, the sample should be in an austenite + ferrite domain. During cooling from 1,200°C, $Cr_{23}C_6$ carbide was formed from the δ-ferrite with its consequent impoverishment in carbon and chromium. Therefore, the martensite formed has low
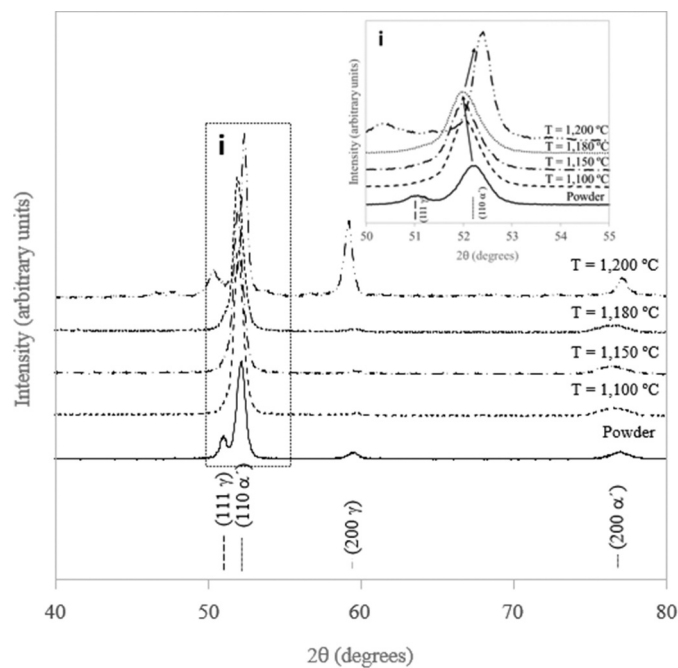
Figure 7. XRD patterns of the sintered samples. the diffractogram of the initial powder is also shown for comparison.

Table 3. Density of the sintered samples.

	420SS_1,100	420SS_1,150	420SS_1,180	420SS_1,200
Density (g/cm³)	7.49	7.52	7.45	7.67
Densification (%)	96.9	97.3	96.4	99.2
Theoretical density (g/cm³)	7.73			

carbon, tending toward the bcc structure of ferrite. This result is in accordance with the work of Abdelkrim Redjaïmia and Antonio Garcia[19] in which the precipitation of $M_{23}C_6$ carbides during anisothermal cooling of a duplex 2205 stainless steel was observed.

Densification

Table 3 shows the density of the sintered samples. The values grow with the increasing sintering temperature with a maximum value of 7.67 g/cm³ for *420SS_1,200* sample (99.2% of densification).

Fracture and hardness

The fracture surface of the sintered samples is shown in Fig. 8. All the samples show a mix of intergranular (cracks propagate along the weakened grain boundaries) and transgranular (cracking propagation inside the grain) fractures. The result of the latter fracture mode is a smooth-looking fracture. Dimples were not detected on any of the fracture surfaces, so it can be stated that the samples are predominantly fragile.

The variation in the hardness runs from the periphery to the center of the four samples and is presented in Fig. 9. In this figure, an optical image of one of the indentations is also shown. A tendency for the hardness to increase from the periphery to the center of the samples was observed. This may be explained either by the decrease in the grain size along the radius or by the existing porosity. Densification is affected by temperature (diffusion), and pressure (plastic deformation). For the lower temperatures, a higher porosity was observed at the periphery of the samples than in the center (Fig. 4). This is due to the particle-wall mold friction that leads to a less efficient sintering process at the periphery of the samples. The average hardness values obtained from 10 indentations with a load of 1,000 gf at different points on the surface of the samples were 601 ± 7, 687 ± 12, 672 ± 8, and 717 ± 5 HV, for the sintering temperatures of 1,100, 1,150, 1,180, and 1,200°C, respectively. These values are lower than the ones obtained from lower applied loads due to the indentation load/size effect. The higher the applied load is, the lower the hardness measured.

The decrease in hardness observed from 1,100 to 1,180°C is explained by the increase in grain size. The highest hardness value was obtained for the sample sintered at 1,200°C, probably due to the formation of chromium carbides during cooling.

The hardness values obtained in this study are higher than those indicated in the literature for the same steel fabricated by most of the processing techniques but are of the same order of magnitude as those of parts printed by SLM (Table 4).

The hardness of the 420 stainless steel is highly dependent on the microstructure (type of phases and their relative amount). In the annealed state this steel is formed by a ferrite + chromium carbide structure with a hardness of around 250 HV.[20,21] Wrought 420 stainless steel quenched and tempered is formed by martensite and retained austenite with a hardness of 567 HV (53 HRC).[10,22] In the study by Nachum et al.[8] a hardness of 550 HV is reported for the 420 stainless steel hot-pressed at 960°C using mechanically milled
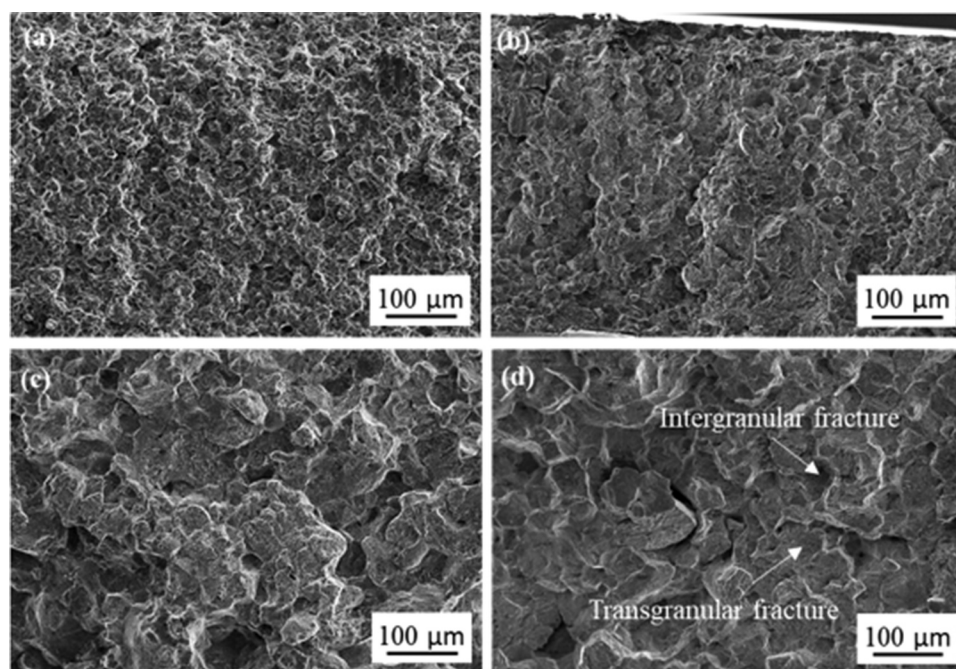
Figure 8. Fracture surface of different samples: (a) 420SS_1,100, (b) 420SS_1,150, (c) 420SS_1,180 and (d) 420SS_1,200.
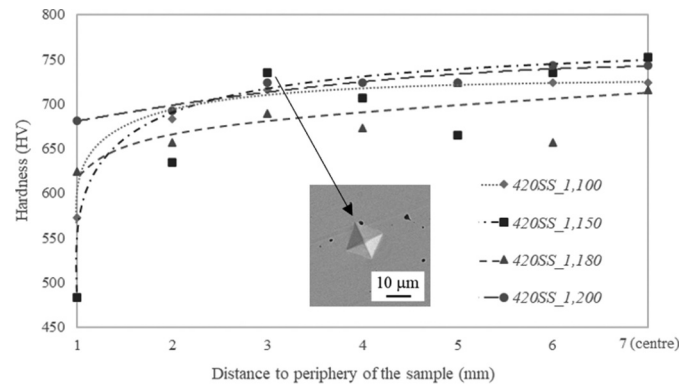
Figure 9. Hardness along the radius of the sintered samples.

Table 4. Hardness of the 420 stainless steel material processed by different techniques.

Process	Hardness (HV)	Reference
Wrought (annealed)	247	20,21
Wrought (quenched and tempered)	567	10,22
HP	550	8
SLM (as-printed)	649	10
SLM (tempered at 315°C)	567	10
SLM (as-printed)	650	1
SLM (tempered at 400°C)	500	1
MIM	490	23
MIM (HT)	497	23
UHSS (CR + AC)	486	24
UHSS (TMCP)	532	24

HP: hot pressing; SLM: selective laser melting; MIM: metal injection molding; HT: heat treated; UHSS: ultra-high strength steel sheets; CR + AC: cold rolling/air cooled; TMCP: thermomechanical controlled processing.

powders. In a recent study, Nath et al.[10] used the selective laser melting (SLM) technique to print a 420 stainless steel part. The authors reported hardness values of 649 HV (55 HRC) and 567 HV (53 HRC) for the as-printed and 315°C tempered samples, respectively, and stated that the heat-treatment did not induce an important change in the retained austenite content within a degree of experimental error of $20 \pm 10\%$. However, the formation of $Cr_{23}C_6$ carbides is stated to occur during tempering. In the Saeidi et al.[1] work, a martensitic 420 stainless steel part was also fabricated by SLM with a microstructure consisting of martensite +11% of retained austenite and a hardness of 650 HV. Tempering at 400°C led to a decrease in hardness (500 HV). The findings in the present study are superior to the hardness of the SLM 420 stainless steel, most likely due to the low percentage of retained austenite achieved (Fig. 7). The same conclusion can be drawn regarding this steel obtained by other production techniques. According to MPIF 35, the hardness of the tempered 420 stainless steel fabricated by metal injection molding (MIM) is 490 HV (48 HRC).[23] Chen et al.[24] measured the hardness of an ultra-high-strength 420 stainless steel processed by cold rolling plus air cooling (CR + AC) and laboratory thermo-mechanical controlled processing (TMCP). The microstructure reported was bainite for the former process and a mixture of lath martensite and bainite for the latter, with hardness of 486 and 532 HV, respectively.

Conclusions

The following conclusions can be drawn from this study:

- Quite dense 420 stainless steel samples were produced by hot pressing at sintering temperatures from 1,100 and 1,200°C. 99.2 % of densification was achieved for the samples sintered at 1,200°C.
- An increase in the sintering temperature led to an increase in the grain size.
- The samples sintered at 1,100, 1,150, and 1,180°C were formed by martensite and austenite. Precipitation of chromium carbides ($Cr_{23}C_6$) occurred in the sample sintered at 1,200°C. This sample presented the highest hardness value.
- Porosity, grain size, and hardness were found to vary along the radius of the samples.

Acknowledgments

Disclosure statement

No potential conflict of interest was reported by the author(s).

ORCID

A. Cunha http://orcid.org/0000-0003-0610-6255
A. Marques http://orcid.org/0000-0001-5418-3453
M. Gasik http://orcid.org/0000-0002-5782-7987
B. Trindade http://orcid.org/0000-0003-2971-8465

References

[1] Saeidi, K.; Zapata, D. L.; Lofaj, F.; Kvetkova, L.; Olsen, J.; Shen, Z.; Akhtar, F. Ultra-High Strength Martensitic 420 Stainless Steel with High Ductility. *Addit. Manuf.* 2019, *29*, 100803. DOI: 10.1016/j.addma.2019.100803.

[2] Momenzadeh, N.; Nath, S. D.; Berfield, T. A.; Atre, S. V. In situ Measurement of Thermal Strain Development in 420 Stainless Steel Additive Manufactured Metals. *Exp. Mech.* 2019, *59*(10), 819–827. DOI: 10.1007/s11340-019-00513-3.

[3] Yadroitsev, I.; Krakhmalev, P.; Yadroitsava, I. Hierarchical Design Principles of Selective Laser Melting for High Quality Metallic Objects. *Addit. Manuf.* 2015, *7*, 45–56. DOI: 10.1016/j.addma.2014.12.007.

[4] Shi, Y.; Xiong, X.; Liu, Z.; Yang, Y.; Hou, J.; Wu, S.; Rao, J. H.; Zhang, K.; Huang, A. Mechanical Property Evaluation of a Slmed Martensitic Stainless Steel. *Acta Metall. Sin.* 2020, *33*(11), 1466–1476. DOI: 10.1007/s40195-020-01128-7.

[5] Nath, S. D.; Gupta, G.; Kearns, M.; Gulsoy, O.; Atre, S. V. Effects of Layer Thickness in Laser-Powder Bed Fusion of 420 Stainless Steel. *Rapid Prototyp. J.* 2020, *26*(7), 1197–1208. DOI: 10.1108/RPJ-10-2019-0279.

[6] Nath, S. D.; Clinning, E.; Gupta, G.; Wuelfrath-Poirier, V.; L'Espérance, G.; Gulsoy, O.; Atre, S. V. Effects of Nb and Mo on the Microstructure and Properties of 420 Stainless Steel Processed by Laser-Powder Bed Fusion. *Addit. Manuf.* 2019, *28*(1), 682–691. DOI: 10.1016/j.addma.2019.06.016.

[7] Nath, S. D.; Okello, A.; Kelkar, R.; Gupta, G.; Kearns, M.; Atre, S. V. Adapting L-PBF Process for Fine Powders: A Case Study in 420 Stainless Steel. *Mater. Manuf. Process.* 2021, 1–12. doi:10.1080/10426914.2021.1885707.

[8] Nachum, S.; Fleck, N. A. The Microstructure and Mechanical Properties of Ball-Milled Stainless Steel Powder: The Effect of Hot-Pressing Vs. Laser Sintering. *Acta Mater.* 2011, *59*(19), 7300–7310. DOI: 10.1016/j.actamat.2011.08.004.

[9] Klar, E., and Samal, P. K. *Powder Metallurgy Stainless Steels: Processing, Microstructure, and Properties*, Ohio: ASM International: 2007; Klar, E., and Samal, P. K. Eds.

[10] Nath, S. D.; Irrinki, H.; Gupta, G.; Kearns, M.; Gulsoy, O.; Atre, S. Microstructure-Property Relationships of 420 Stainless Steel Fabricated by Laser-Powder Bed Fusion. *Powder Technol.* 2019, *343*(1), 738–746. DOI: 10.1016/j.powtec.2018.11.075.

[11] Gupta, R. K.; Kumar, V. A.; Khanra, G. P. 2017. Reactive and Liquid-Phase Sintering Techniques. In *Intermetallic Matrix Composites: Properties and Applications*, Mitra, R., Ed., pp. 303–318. Woodhead Publishing: doi:10.1016/B978-0-85709-346-2.00011-X.

[12] Eray, S. 2020. Application of Metal Oxides in Composites. In *Metal Oxide Powder Technologies*, Al-Douri, Y., Ed., pp. 101–119. Elsevier: doi:10.1016/B978-0-12-817505-7.00006-3.

[13] Balamurugan, P.; Uthayakumar, M. Influence of Process Parameters on Cu-Fly Ash Composite by Powder Metallurgy Technique. *Mater. Manuf. Process.* 2015, *30*(3), 313–319. DOI: 10.1080/10426914.2014.984220.

[14] Bolzoni, L.; Ruiz-Navas, E. M.; Gordo, E. Quantifying the Properties of Low-Cost Powder Metallurgy Titanium Alloys. *Mater. Sci. Eng. A* 2017, *687*, 47–53. DOI: 10.1016/j.msea.2017.01.049.

[15] Beri, N.; Maheshwari, S.; Sharma, C.; Kumar, A. Technological Advancement in Electrical Discharge Machining with Powder Metallurgy Processed Electrodes: A Review. *Mater. Manuf. Process.* 2010, *25*(10), 1186–1197. DOI: 10.1080/10426914.2010.512647.

[16] Sahoo, S.; Jha, B. B.; Sahoo, T. K.; Mandal, A. Influence of Reinforcement and Processing on Steel-Based Composites: Microstructure and Mechanical Response. *Mater. Manuf. Process.* 2018, *33*(5), 564–571. DOI: 10.1080/10426914.2017.1364865.

[17] Miranda, G.; Araújo, A.; Bartolomeu, F.; Buciumeanu, M.; Carvalho, O.; Souza, J. C. M.; Silva, F. S.; Henriques, B. Design of Ti6al4v-HA Composites Produced by Hot Pressing for Biomedical Applications. *Mater. Des.* 2016, *108*, 488–493. DOI: 10.1016/j.matdes.2016.07.023.

[18] Barlow, L. D.; Du Toit, M. Effect of Austenitizing Heat Treatment on the Microstructure and Hardness of Martensitic Stainless Steel AISI 420. *J. Mater. Eng. Perform.* 2012, *21*(7), 1327–1336. DOI: 10.1007/s11665-011-0043-9.

[19] Redjaïmia, A.; Garcia, A. M. M. On the M23C6-Carbide in 2205 Duplex Stainless Steel: An Unexpected (M23c6/austenite) - Eutectoid in the δ-Ferritic Matrix. *Metals (Basel).* 2021, *11*(9), 1340. DOI: 10.3390/met11091340.

[20] Sealy, M. P.; Hadidi, H.; Sotelo, L. D.; Li, W. L.; Turner, J. A.; McGeough, J. A. Compressive Behavior of 420 Stainless Steel After Asynchronous Laser Processing. *CIRP Ann.* 2020, *69*(1), 169–172. DOI: 10.1016/j.cirp.2020.04.059.

[21] Haghdadi, N.; Laleh, M.; Moyle, M.; Primig, S. Additive Manufacturing of Steels: A Review of Achievements and Challenges. *J. Mater. Sci.* 2021, *56*(1), 64–107. DOI: 10.1007/s10853-020-05109-0.

[22] Tian, Y.; Chadha, K.; Aranas, C. Laser Powder Bed Fusion of Ultra-High-Strength 420 Stainless Steel: Microstructure Characterization, Texture Evolution and Mechanical Properties. *Mater. Sci. Eng. A* 2021, *805*, 140790. DOI: 10.1016/j.msea.2021.140790.

[23] MPIF Standard 35. Materials Standards for PM Structural Parts;Metal Powder Industries Federation, Princeton, NJ. 2016, pp 32–35.

[24] Chen, L.; Huang, J.; Zhao, Y.; Di, H.; Zhu, F. P. Microstructures and Mechanical Properties of Ultra-High Strength Steel Sheet. *Procedia. Eng.* 2014, *81*, 84–89. DOI: 10.1016/j.proeng.2014.09.131.